Efficiency Improvement of Three Port High Frequency Transformer Isolated Triple Active Bridge Converter

Ritwik Chattopadhyay[a], Ghanshyamsinh Gohil[b], Sayan Acharya[a], Viju Nair[a] and Subhashish Bhattacharya[a]
[a]Department of Electrical and Computer Engineering, North Carolina State University, Raleigh, NC, USA.
[b]Department of Electrical and Computer Engineering, University of Texas at Dallas, TX, USA.

***Abstract*—This paper discusses and compares few techniques for efficiency improvement of Three-port Triple Active Bridge(TAB) Converter. Transformer isolated three port phase shifted Triple Active Bridge dc-dc converters are very efficient in nature providing high efficiency, ZVS operation over wide range, galvanic isolation and bidirectional power flow capability. The natural turn-on ZVS for switching devices in DAB or TAB converters is a very useful property for using Mosfets, as it reduces the device losses by a huge margin. The natural ZVS is lost for phase shifted converters at low power operating regions, causing reduction in efficiency. This paper discusses a comparsion between phase shift operation at fixed frequency vs phase shift operation at varying frequency and varying duty cycle operation at fixed frequency, which leads to a greater operating range of natural turn-on ZVS thus improving the efficiency. A comparison of the three methods have been presented in this paper with experimental results from a 10kW hardware prototype made of SiC Mosfets.**

***Keywords*—Phase Shifted Converter, Triple Active Bridge, ZVS turn-on, SiC MOSFET, Efficiency Improvement**

I. Introduction

Integrating large scale(few MWs) Renewable Energy Sources(RES) into grid, is a challenging task and it requires efficient and reliable converters. Moreover, Renewable Energy Sources like PV or Wind has intermittent power fluctuations which require some form of Energy Storage Systems(ESS) to support the power fluctuations. The integration of energy storage is an interesting topic of research as the integration can be carried out at modular building block level, where the ESS is integrated with RES at a lower power level. The second method to integrate ESS is to use a separate high power converter in parallel to RES converter for grid integration. In this paper, the method of integrating RES with ESS at modular level is discussed, since it presents the advantage of reducing the power fluctuations at building block level.

Phase shifted dc-dc converters[1]-[5] have been very interesting topic of research in power electronics. The phase shifted dc-dc converters provide the advantages of bidirectional power flow capability, natural ZVS turn-on, high efficiency, wide range of operating voltages. In this paper, a three port Triple Active Bridge(TAB) converter(figure 1) is used for integrating Renewable Energy Sources(RES) and Energy Storage Systems(ESS),[5],[8]-[11]. The natural turn-on of switching devices in DAB or TAB converter provides high efficiency. The natural ZVS turn-on is a very desired property for switching SiC Mosfets as they have significant amount of switching losses during turn-on, with two components of switching losses (a)switching loss due to rising device current and falling device voltage, (b) discharge of charge held by device capacitance C_{ds} in the device channel[6][7]. The hard switching turn-off of SiC-Mosfets have very low loss actually taking place during the turn-off as most of the turn-off energy is stored in device capacitance C_{ds}. Hence, achieving a natural ZVS turn-on in SiC-Mosfets reduces the switching loss by huge margin and provides the flexibility to designers for opting higher switching frequency for the high frequency transformer. However, the natural turn-on ZVS for switching Mosfets depends on the direction and magnitude of line current during turn-off, device capacitance and line inductance. From [10],[12], the ZVS is achieved at higher line currents at mid-to-high power operating regions. At low power operating regions, the ZVS is drastically lost due to loss of natural turn-on ZVS with reduction of operating power level, resulting in decrease of line current.

In this paper, two methods are used to investigate the efficiency improvement of Triple Active Bridge(TAB) converter by extending the ZVS operating range. TAB converters are generally operated with square wave voltages with 50% duty cycle or with quasi-square wave voltages with less than 50% duty cycle. The first method includes increasing the switching frequency of the converter, so that higher phase angle is required for power transfer, leading to high winding current and ZVS. The second method uses duty cycle variation with fixed frequency. Lower duty cycle requires high phase shift angles, leading to higher line current, thus enabling the ZVS operation. In this paper, the two methods are compared against a 50% duty cycle operation at fixed frequency. The efficiency comparison is carried out for a 10kW SiC Mosfet based prototype with a high frequency transformer designed for 50kHz operating frequency.

II. Three Port Phase Shifted Converter Analysis for Square Wave Winding Voltages

A. Piecewise Linear Model& Average Power for Three Port Transformer

The three port phase shifted Triple active Bridge(TAB) converter is operated using phase shifted voltages for different windings. The converter mentioned in figure 1, uses a high frequency transformer which has considerable leakage inductance

978-1-5386-1180-7/18/$31.00 ©2018 IEEE

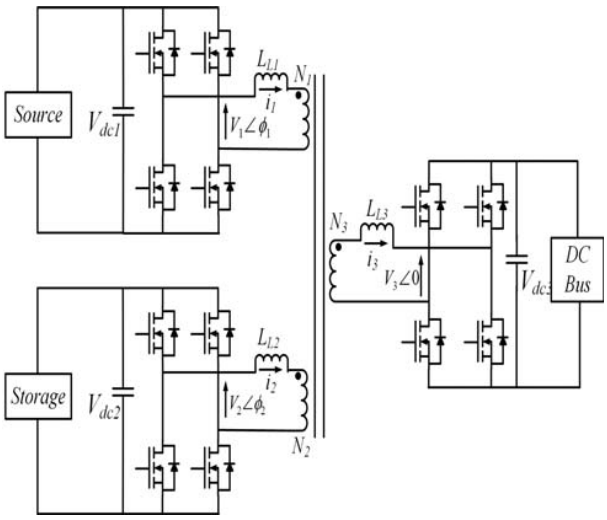

Fig. 1: Triple Active Bridge(TAB) Phase-Shifted DC-DC Converter

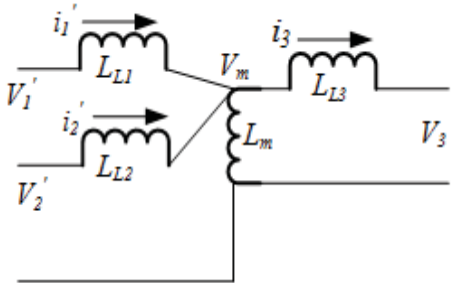

Fig. 2: Equivalent Circuit of Transformer for TAB Converter

for power transfer and no series inductance is required. The equivalent circuit of the high frequency transformer is shown in figure 2. The power transfer is dependent upon voltage magnitudes, phase shift angles and leakage inductances of the high frequency transformer. The leakage inductances for the winding high frequency transformer, act as energy transferring elements[1]-[5],[8]-[12]. The different power flow cases for the three port converter of figure 1, can be described by the phase shift angle magnitudes and directions. In figure 1, the voltage V_3 is considered as the reference voltage and the other two winding voltages V_1,V_2 are positioned at phase angles ϕ_1,ϕ_2.

The transformer winding currents for phase shifted TAB converter, with square wave winding voltages, can be modeled using piecewise linear nature of the winding currents. The piecewise linear model of the winding currents are functions of phase shift angles ϕ_1 and ϕ_2. For this paper, it is assumed that RES at port 1 acts as source and can only deliver power, while the ESS at port 2 can act as both source and sink. The three possible scenarios based on the phase shift angles are depicted as (a) $-\phi_1 < -\phi_2 < 0$, (b) $-\phi_2 < -\phi_1 < 0$, and (c) $-\phi_1 < 0 < \phi_2$, as shown in figures 3-5.

In order to realize the winding currents and the power

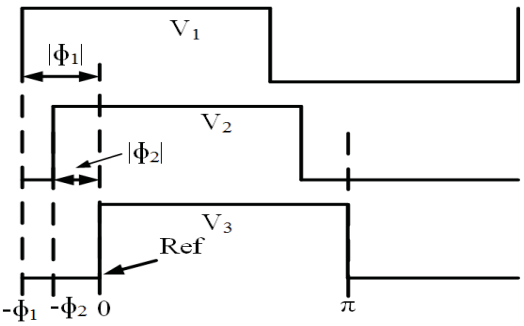

Fig. 3: Mode 1: Winding Voltages when $-\phi_1 < -\phi_2 < 0$

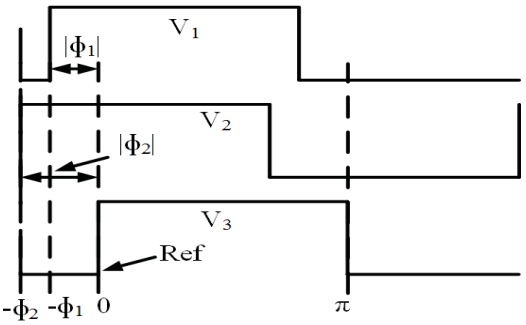

Fig. 4: Mode 2: Winding Voltages when $-\phi_2 < -\phi_1 < 0$

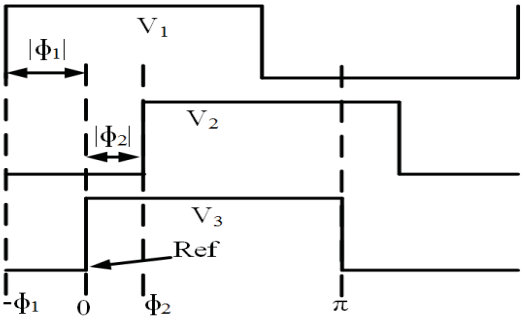

Fig. 5: Mode 3: Winding Voltages when $-\phi_1 < 0 < \phi_2$

flow expressions for the converter, the voltage V_{m1} across the magnetizing inductance L_m, referred to windings 1,2,3 are given in equations (1,2,3). The voltage term V_{xy} is used to refer to the voltage V_x referred to winding y. Similarly, inductance L_{Lxy} is used to refer to inductance L_{Lx} referred to winding y. The piecewise linear nature of the currents for windings 1,2 and 3 are given in equations (7-9). In these equations, $'\theta_0'$ is initial instant for the linear interval x, $'\theta'$ is any instant within

that interval x and ${m_x}^y$ is slope of interval x for winding y.

$$V_{m1} = \left[\frac{(V_1 L_{L21} L_{L31} + V_{21} L_{L1} L_{L31} + V_{31} L_{L21} L_{L1}) L_{m1}}{{L_{n1}}^3} \right] \tag{1}$$

$$V_{m2} = \left[\frac{(V_2 L_{L12} L_{L32} + V_{12} L_{L2} L_{L32} + V_{32} L_{L2} L_{L12}) L_{m2}}{{L_{n2}}^3} \right] \tag{2}$$

$$V_{m3} = \left[\frac{(V_{13} L_{L23} L_{L3} + V_{23} L_{L13} L_{L3} + V_3 L_{L23} L_{L13}) L_{m3}}{{L_{n3}}^3} \right] \tag{3}$$

where

$${L_{n1}}^3 = L_{L1} L_{L21} L_{L31} + L_{L1} L_{L21} L_{m1} + L_{L1} L_{L31} L_{m1} + L_{L21} L_{L31} L_{m1} \tag{4}$$

$${L_{n2}}^3 = L_{L12} L_{L2} L_{L32} + L_{L12} L_{L2} L_{m2} + L_{L12} L_{L32} L_{m2} + L_{L2} L_{L32} L_{m2} \tag{5}$$

$${L_{n3}}^3 = L_{L13} L_{L23} L_{L3} + L_{L13} L_{L23} L_{m3} + L_{L13} L_{L3} L_{m3} + L_{L23} L_{L3} L_{m3} \tag{6}$$

$$i_1(\theta) = i_1(\theta_0) + \frac{\{V_1(\theta) - V_{m1}(\theta)\}}{\omega L_{L1}}(\theta - \theta_0) = i_1(\theta_0) + {m_x}^1(\theta - \theta_0) \tag{7}$$

$$i_2(\theta) = i_2(\theta_0) + \frac{\{V_2(\theta) - V_{m2}(\theta)\}}{\omega L_{L2}}(\theta - \theta_0) = i_2(\theta_0) + {m_x}^2(\theta - \theta_0) \tag{8}$$

$$i_3(\theta) = i_3(\theta_0) + \frac{\{V_{m3}(\theta) - V_3(\theta)\}}{\omega L_{L3}}(\theta - \theta_0) = i_3(\theta_0) + {m_x}^3(\theta - \theta_0) \tag{9}$$

The derived power flow expressions in the above equations, reveal that the three port system is a coupled system and power flow of one port is coupled to the power flowing of the other two ports flow of one port cannot be controlled using one phase angle. The power flow control for this kind of system has been discussed in [5][11][12]. The instantaneous current expressions during switching instants are given in equations (10-18), where the parameters ${K_x}^y$ are functions of inductances during piecewise linear interval x for winding current y.

$$i_1(-\phi_1) = -V_{dc1}{K_1}^1\pi + V_{dc2}{K_2}^1(\pi - 2|\phi_{12}|) + V_{dc3}{K_3}^1(\pi - 2|\phi_1|) \tag{10}$$

$$i_1(-\phi_2) = -V_{dc1}{K_1}^1(\pi - 2|\phi_{12}|) + V_{dc2}{K_2}^1\pi + V_{dc3}{K_3}^1(\pi - 2|\phi_2|) \tag{11}$$

$$i_1(0) = -V_{dc1}{K_1}^1(\pi - 2|\phi_1|) + V_{dc2}{K_2}^1(\pi - 2|\phi_2|) + V_{dc3}{K_3}^1\pi \tag{12}$$

$$i_2(-\phi_1) = -V_{dc2}{K_1}^1(\pi - 2|\phi_{12}|) + V_{dc1}{K_2}^2\pi + V_{dc3}{K_3}^2(\pi - 2|\phi_1|) \tag{13}$$

$$i_2(-\phi_2) = -V_{dc2}{K_1}^2\pi + V_{dc1}{K_2}^2(\pi - 2|\phi_{12}|) + V_{dc3}{K_3}^2(\pi - 2|\phi_2|) \tag{14}$$

$$i_2(0) = -V_{dc2}{K_1}^2(\pi - 2|\phi_2|) + V_{dc1}{K_2}^2(\pi - 2|\phi_1|) + V_{dc3}{K_3}^2\pi \tag{15}$$

$$i_3(-\phi_1) = V_{dc3}{K_1}^3(\pi - 2|\phi_1|) - V_{dc1}{K_2}^3\pi - V_{dc2}{K_3}^c(\pi - 2|\phi_{12}|) \tag{16}$$

$$i_3(-\phi_2) = V_{dc3}{K_1}^3(\pi - 2|\phi_2|) - V_{dc1}{K_2}^3(\pi - 2|\phi_{12}|) - V_{dc2}{K_3}^2\pi \tag{17}$$

$$i_3(0) = V_{dc3}{K_1}^3\pi - V_{dc1}{K_2}^3(\pi - 2|\phi_1|) - V_{dc2}{K_3}^2(\pi - 2|\phi_2|) \tag{18}$$

The average power flow for each port of the three port TAB converter of figure 1, can be expressed by product of half cycle average voltage and half cycle average current. Using square wave voltage pattern, the half cycle average voltage is equal to the corresponding dc link voltage for each port and the half cycle average currents are obtained by averaging the linear models from equations (7-9). The average dc power flow over a switching cycle for each port are given below in equations (10-12). The turns ratio term r_{xy} is defined as $r_{xy} = \frac{N_x}{N_y}$, where N_x, N_y are number of turns for windings x, y.

$$P_1 = \frac{V_{dc1} r_{13} V_{dc3} \phi_1 (\pi - |\phi_1|) L_{L21} L_{L31}}{\pi \omega {L_{n1}}^3} + \frac{V_{dc1} r_{12} V_{dc2} (\phi_1 - \phi_2)(\pi - |\phi_1 - \phi_2|) L_{L31} L_{m1}}{\pi \omega {L_{n1}}^3} \tag{19}$$

$$P_2 = \frac{V_{dc2} r_{23} V_{dc3} \phi_2 (\pi - |\phi_2|) L_{L12} L_{L32}}{\pi \omega {L_{n2}}^3} - \frac{r_{21} V_{dc1} V_{dc2} (\phi_1 - \phi_2)(\pi - |\phi_1 - \phi_2|) L_{L32} L_{m2}}{\pi \omega {L_{n2}}^3} \tag{20}$$

$$P_3 = \frac{r_{31} V_{dc1} V_{dc3} \phi_1 (\pi - |\phi_1|) L_{L23} L_{L3}}{\pi \omega {L_{n3}}^3} + \frac{r_{32} V_{dc2} V_{dc3} \phi_2 (\pi - |\phi_2|) L_{L13} L_{L3}}{\pi \omega {L_{n3}}^3} \tag{21}$$

B. Core Loss Modelling for Three Port Transformer

The core loss model for three port transformer is derived here using iGSE method[13] as a function of operating phase shift angles ϕ_1 and ϕ_2. For the three port converter of figure 1, the core flux depends on the voltage V_m, which depends on the phase shift angles. The voltage V_m is expressed a discontinuous function of ϕ_1 and ϕ_2 over a switching period, however each half cycle can be divided into three continuous sub intervals which are defined as (a) $-\phi_1 < -\phi_2 < 0$, (b) $-\phi_2 < -\phi_1 < 0$, and (c) $-\phi_1 < 0 < \phi_2$. The expression for core loss per unit volume using iGSE method, between any two instants γ_1 and γ_2 is given in equation (22). The $\frac{dB}{dt}$ and ΔB are evaluated as functions of different system parameters for each of the continuous linear interval between 0 to π based

on the operating phase shift angles. The ferrite core loss per unit volume for each of the three cases mentioned above are given in equations (23)-(25).

$$P_v(\gamma_1,\gamma_2) = \frac{1}{\pi}\int_{\gamma_1}^{\gamma_2} k_i \left|\frac{dB}{dt}\right|^{\alpha} (\Delta B)^{\beta-\alpha} d\theta \tag{22}$$

$$Case1 : \phi_1 > \phi_2 > 0$$
$$\begin{aligned} P_{core} =& P_v(0, \pi - |\phi_1|) + P_v(\pi - |\phi_1|, \pi - |\phi_1|) \\ &+ P_v(\pi - |\phi_1|, \pi) \end{aligned} \tag{23}$$

$$Case2 : \phi_2 > \phi_1 > 0$$
$$\begin{aligned} P_{core} =& P_v(0, \pi - |\phi_2|) + P_v(\pi - |\phi_2|, \pi - |\phi_1|) \\ &+ P_v(\pi - |\phi_1|, \pi) \end{aligned} \tag{24}$$

$$Case3 : \phi_1 > 0 > -\phi_2$$
$$\begin{aligned} P_{core} =& P_v(0, |\phi_2|) + P_v(|\phi_2|, \pi - |\phi_1|) \\ &+ P_v(\pi - |\phi_1|, \pi) \end{aligned} \tag{25}$$

C. Device Conduction Loss & Copper Losses for Three Port Converter with Square Wave Winding Voltages

The three port converter of figure 1 has conduction losses resulting from Mosfet on-state resistance R_{ds} and from transformer copper losses. The conduction loss for devices and copper losses for transformers are expressed here using harmonic model of the winding currents. Harmonic components of each winding current is derived using the fourier coefficients for the winding currents. The square of the peak value of n^{th} harmonic component of the k^{th} winding current is shown in equation (26). The total copper loss for the three port transformer is sum of conduction losses for each harmonic component of currents in the three windings. In this paper, upto 7^{th} harmonic component is considered for copper losses. The device conduction loss for the converter can be expressed as sum of conduction losses for all the three converters. The RMS current of each device for a H-bridge is $1/\sqrt{2}$ times of RMS value of winding current for that harmonic component. Henceforth, the device conduction losses are evaluated using the winding current expression for the high frequency transformer.

$${I_{kn}}^2 = \frac{4}{\pi^2}[(\int_0^{\pi} i(\theta)\cos(n\theta)d\theta)^2 + (\int_0^{\pi} i(\theta)\sin(n\theta)d\theta)^2] \tag{26}$$

$$P_{cu} = \sum_{k=1}^{3}(\sum_{n=1}^{7}(\frac{I_{kn}}{\sqrt{2}})^2 R_{kn,ac}) \tag{27}$$

$$P_{device} = \sum_{k=1}^{3}(4(\sum_{n=1}^{7}(\frac{I_{kn}}{2})^2))R_{ds} \tag{28}$$

III. Three Port Phase Shifted Converter Analysis for Quasi-Square Wave Winding Voltages

A. Harmonic Model Based Winding Currents & Average Power for Three Port Transformer

In this section, analysis for operation of three port phase shifted Triple Active Bridge(TAB) converter using quasi-square wave voltages or square wave voltages with zero voltage duration, is presented. The equivalent circuit of TAB converter, mentioned in figure 1, represents a detailed circuit for three port transformer. In this section, a reduced model of the equivalent circuit is used, which is obtained by considering the magnetizing inductance $L_m >> L_{L1}, L_{L2}, L_{L3}$ and converting the star connection of leakage inductances into a delta connection as shown in figure 6. The equivalent inductances of delta connection can be obtained by converting the leakage inductances in delta form. A typical transformer winding voltages and currents waveform for quasi-square wave voltage operation is shown in figure 7.

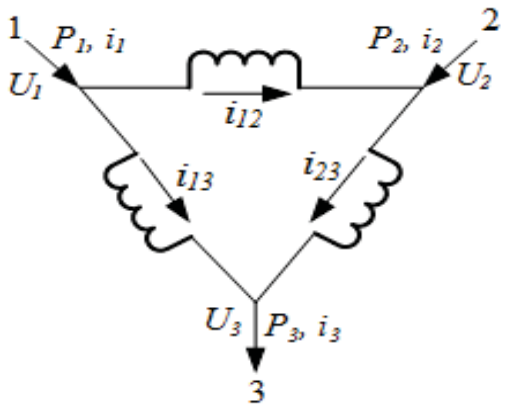

Fig. 6: Equivalent Circuit of Delta Connected

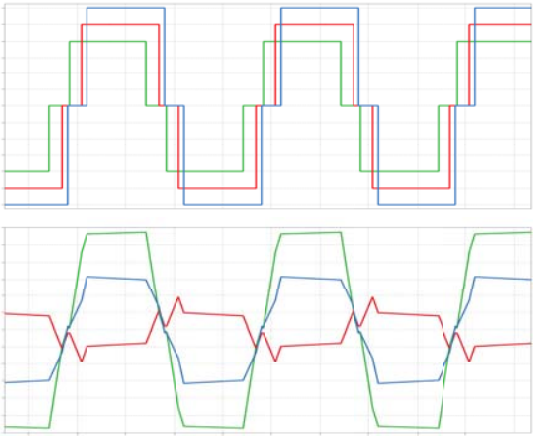

Fig. 7: Transformer Winding Voltages and Currents

The winding voltage expressions using harmonic model for each port with quasi-square voltage waveforms are given in equations (29)-(31). The three winding currents are derived here using the winding voltage harmonics. The harmonic current vector expressions for any harmonic component 'n', using the voltage vectors, are shown in equations (32)-(34).

The active power flow expressions for each port are dervied over a switching cycle and are expressed in (35)-(37). The current expressions in vector form are derived in terms of different parameters, and are given in equations(38)-(40). The RMS current expressions are shown in equations (41)-(43).

$$u_1(\omega t) = \sum_{n=1}^{7} \frac{4V_{dc1}}{n\pi} \sin(\frac{nD_1\pi}{2}) \sin(n\omega t + n\phi_1) = \sum_{n=1}^{7} \sqrt(2)U_{1n} \sin(n\omega t + n\phi_1) \tag{29}$$

$$u_2(\omega t) = \sum_{n=1}^{7} \frac{4V_{dc2}}{n\pi} \sin(\frac{nD_2\pi}{2}) \sin(n\omega t + n\phi_2) = \sum_{n=1}^{7} \sqrt(2)U_{2n} \sin(n\omega t + n\phi_2) \tag{30}$$

$$u_3(\omega t) = \sum_{n=1}^{7} \frac{4V_{dc3}}{n\pi} \sin(\frac{nD_3\pi}{2}) \sin(n\omega t) = \sum_{n=1}^{7} \sqrt(2)U_{3n} \sin(n\omega t) \tag{31}$$

$$I_{1n} = \frac{U_{1n}\angle n\phi_1 - U_{2n}\angle n\phi_2}{n\omega L_{12}} + \frac{U_{1n}\angle n\phi_1 - U_{3n}\angle 0}{n\omega L_{13}} \tag{32}$$

$$I_{2n} = \frac{U_{2n}\angle n\phi_2 - U_{1n}\angle n\phi_1}{n\omega L_{12}} + \frac{U_{2n}\angle n\phi_2 - U_{3n}\angle 0}{n\omega L_{23}} \tag{33}$$

$$I_{3n} = \frac{U_{1n}\angle n\phi_1 - U_{3n}\angle 0}{n\omega L_{13}} + \frac{U_{2n}\angle n\phi_2 - U_{3n}\angle 0}{n\omega L_{23}} \tag{34}$$

$$P_1 = \sum_{n=1}^{7} (\frac{U_{1n}U_{2n}\sin n\phi_{12}}{n\omega L_{12}} + \frac{U_{1n}U_{3n}\sin n\phi_{13}}{n\omega L_{13}}) \tag{35}$$

$$P_2 = \sum_{n=1}^{7} (-\frac{U_{1n}U_{2n}\sin n\phi_{12}}{n\omega L_{12}} + \frac{U_{2n}U_{3n}\sin n\phi_{23}}{n\omega L_{23}}) \tag{36}$$

$$P_3 = \sum_{n=1}^{7} (\frac{U_{1n}U_{3n}\sin n\phi_{13}}{n\omega L_{13}} + \frac{U_{2n}U_{3n}\sin n\phi_{23}}{n\omega L_{23}}) \tag{37}$$

$$\begin{aligned} I_{1n} &= [\frac{U_{1n}\sin(n\phi_1)}{n\omega L_{13}} + \frac{U_{1n}\sin(n\phi_1)}{n\omega L_{12}} - \frac{U_{2n}\sin(n\phi_2)}{n\omega L_{12}}] \\ &+ j[\frac{U_{3n}}{n\omega L_{13}} + \frac{U_{2n}\cos(n\phi_2)}{n\omega L_{12}} \\ &- \frac{U_{1n}\cos(n\phi_1)}{n\omega L_{12}} - \frac{U_{1n}\cos(n\phi_1)}{n\omega L_{13}}] \\ &= A_{1n} + jB_{1n} \end{aligned} \tag{38}$$

$$\begin{aligned} I_{2n} &= [\frac{U_{2n}\sin(n\phi_2)}{n\omega L_{12}} + \frac{U_{2n}\sin(n\phi_2)}{n\omega L_{23}} - \frac{U_{1n}\sin(n\phi_1)}{n\omega L_{12}}] \\ &+ j[\frac{U_{3n}}{n\omega L_{23}} + \frac{U_{1n}\cos(n\phi_1)}{n\omega L_{12}} \\ &- \frac{U_{2n}\cos(n\phi_2)}{n\omega L_{12}} - \frac{U_{2n}\cos(n\phi_2)}{n\omega L_{23}}] \\ &= A_{2n} + jB_{2n} \end{aligned} \tag{39}$$

$$\begin{aligned} I_{3n} &= [\frac{U_{1n}\sin(n\phi_1)}{n\omega L_{13}} + \frac{U_{2n}\sin(n\phi_2)}{n\omega L_{23}}] + j[\frac{U_{3n}}{n\omega L_{13}} \\ &+ \frac{U_{3n}}{n\omega L_{23}} - \frac{U_{1n}\cos(n\phi_1)}{n\omega L_{13}} - \frac{U_{2n}\cos(n\phi_2)}{n\omega L_{23}}] \\ &= A_{3n} + jB_{3n} \end{aligned} \tag{40}$$

$$I_{1,rms}^2 = \sum_{n=1}^{7} ({A_{1n}}^2 + {B_{1n}}^2) \tag{41}$$

$$I_{2,rms}^2 = \sum_{n=1}^{7} ({A_{2n}}^2 + {B_{2n}}^2) \tag{42}$$

$$I_{3,rms}^2 = \sum_{n=1}^{7} ({A_{3n}}^2 + {B_{3n}}^2) \tag{43}$$

B. Core Loss Derivation for Quasi-Square Wave Voltage Waveforms

The core loss for three port transformer is derived here using the steinmetz equation for core loss. An approximate approach of core loss considering only the fundamental component of core flux is considered here. The core flux induced in the transformer core is a function of the voltage V_m induced across the magnetizing inductance L_m of the equivalent circuit of figure 3. The expression of V_m is given in equation (44).

$$V_m = [\frac{u_1}{K_1} + \frac{u_2}{K_2} + \frac{u_3}{K_3}]L^2 \tag{44}$$

where, $K_1 = L_{31}L_{12}, K_2 = L_{32}L_{12}, K_1 = L_{31}L_{12}$, and

$$L = L_{L1}L_{L2} + L_{L1}L_{L3} + L_{L3}L_{L2} \tag{45}$$

Considering only fundamental component, the voltage V_m is given as follows,

$$\begin{aligned} V_m &= [\frac{\sqrt{2}U_{11}\sin(\omega t + \phi_1)}{K_1} + \frac{\sqrt{2}U_{21}\sin(\omega t + \phi_2)}{K_2} \\ &+ \frac{\sqrt{2}U_{31}\sin(\omega t)}{K_3}]L^2 \end{aligned} \tag{46}$$

the peak value of the fundamental is given in equation(47).

$$\begin{aligned} V_{m,peak} &= [\frac{2U_{11}}{{K_1}^2} + \frac{2U_{21}}{{K_2}^2} + \frac{2U_{31}}{{K_3}^2} \\ &+ \frac{4U_{21}U_{31}\cos(\phi_2)}{K_2K_3} + \frac{4U_{11}U_{31}\cos(\phi_1)}{K_1K_3} \\ &+ \frac{4U_{11}U_{21}\cos(\phi_1 - \phi_2)}{K_1K_2}]^{\frac{1}{2}} \end{aligned} \tag{47}$$

The peak value of $V_{m,peak}$ is used to find the peak value of core flux, by considering all the elements from the third port, it can be referred from any other two ports as well. The expression for core loss is derived below.

$$B_{peak} = \frac{V_{m,peak}}{\omega N_3 A_c} \tag{48}$$

$$P_{core} = KB_{peak}^{\alpha} f^{\beta} A_c l_m \tag{49}$$

where f is the operating frequency, $\omega = 2\pi f$, A_c is the cross section of the core and l_m is mean length of magnetic flux path.

C. Copper Loss & Device Conduction losses for Quasi-Square Wave Voltage Waveforms

The copper losses for high frequency transformer and conduction losses for devices are expressed in following equations using the RMS values for winding currents.

$$P_{cu} = \sum_{m=1}^{3} (\sum_{n=1}^{7} (I_{mn})^2 R_{mn,ac}) \tag{50}$$

$$P_{device} = 3 \sum_{m=1}^{3} \sum_{n=1}^{7} 2({I_{mn}}^2) R_{ds} \tag{51}$$

IV. Experimental Study and Discussions

A. Different Operating Methods with ZVS & Minimization of Losses

An experimental study of a 10kW three port converter prototype of figure 1 has been carried out for comparing the system efficiencies for different operating schemes. The comparison has been performed for three types of operating mode (a) Fixed frequency operation with square wave winding voltages, (b) Variable frequency operation with square wave winding voltages and (c) Fixed frequency operation with quasi-square wave winding voltages. The operation of three port phase shifted converter for method (a) with fixed frequency and square wave winding voltages provide unique operating point for every value of reference power flow associated to each port. Hence for method (a), solving the equations (19)-(21) provide the solutions for every operating scenario.

One of the drawback of fixed frequency operation with square wave is at low power scenarios, natural ZVS turn-on of devices is lost due to low transformer winding current, which results into drastic reduction of efficiencies at low power region. In order to improve the efficiency at low power operating region, achieving natural ZVS turn-on for switching devices is important. This can be achieved by method (b), increasing the frequency of the operating winding voltages, so that the phase shift angle required for same power transfer is higher than that required for operation at nominal design frequency. The higher phase shift angle results in higher reactive power and higher winding current, thus extending the ZVS range for the three port converter operation at low power. The second method of increasing the ZVS operating range is to use quasi-square wave voltage waveform, which introduces a zero voltage period in winding voltages, enforcing wider phase angle and higher winding current, resulting in increased ZVS range. However, increasing frequency or reducing duty cycle of winding voltage waveforms, results in change of core loss, copper loss and device conduction loss. Hence, determining optimum switching frequency and optimum values of phase shift angles, duty cycles of winding voltages are necessary.

The turn-on ZVS criteria for any switching leg is explained in [4], where the outgoing current needs to lag the phase voltage. For negative to positive transition of winding voltage for any port, the current flowing into the winding, should have a negative minimum value during the transition instant. The required minimum value of the negative current is given in equation (52), where k is the winding port for which ZVS is evaluated, and C_{ds} is the drain-source device capacitance for the switching device.

$$I_{k,min} = 2\sqrt{\frac{C_{ds}}{L_{Lk}} V_k V_m} \tag{52}$$

The evaluation of optimum switching frequency for three port converter operation with square wave winding voltages, is obtained by varying the frequency over a range and finding the minimum value of system losses over the frequency range. A MATLAB routine is created to evaluate the optimum switching frequency, which uses the core loss, copper loss and device loss models from section 2 to evaluate the total system dominant losses. The ZVS conditions are checked by using the current expressions of (10)-(18) and the ZVS criterion of equation (52).

Evaluation of optimum values of winding voltages' duty cycles are carried out by using the duty cycles D_1, D_2, D_3 as free variables for MATLAB minimization routine 'fmincon'. The minimization routine checks for each combination of the duty cycles over the range of upper bound and lower bound values, solves the operating phase shift angles ϕ_1, ϕ_2 using equations (35)-(37), checks for ZVS conditions, evaluates the total dominant system losses by summing up core loss, copper loss & device conduction loss models from section 3. The ZVS condition is checked using equation (52), where the harmonic components of winding currents are added to get the instantaneous winding current values during transition, as given in equation (53).

$$i_k(\phi_k) = \sum_{n=1}^{7} \sqrt{{A_{kn}}^2 + {B_{kn}}^2} \sin(n\phi_k + \tan^{-1}\frac{B_{kn}}{A_{kn}}) \tag{53}$$

B. Experimental Study for Frequency Improvement

The different operating methods of three port Triple Active Bridge converter mentioned above, are experimentally verified with a 10kW SiC-Mosfet based three port converter. The experimental prototype converter uses 1200V/60A SiC-Mosfets for port 1 & 2, and 1700V/45A SiC-Mosfets for port 3. The three port high frequency transformer used is made of ferrite cores with litz wire. Figure 8 shows one of the three H-bridges for three port converter and figure 9 shows the 50kHz/10kW high frequency transformer.

The converter has been run over 2kW to 10kW power range. The voltages for three port converters are defined as $V_{dc1} = V_{dc2} = 800V$, $V_{dc3} = 1200V$. The frequency range chosen for frequency variation method is from 50kHz to 100kHz. The duty cycle range chosen for the quasi-square wave winding voltage waveforms, is from 0.7 to 1. Figures (10)-(13) show the transformer winding voltages and currents for different cases.

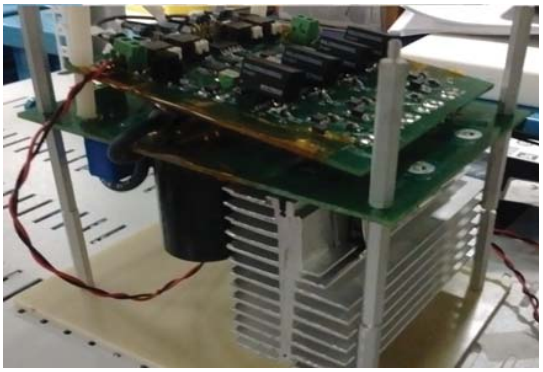

Fig. 8: 1200V/1700V H-bridge Converter Prototype

Fig. 9: 10kW/50kHz Three Port Transformer

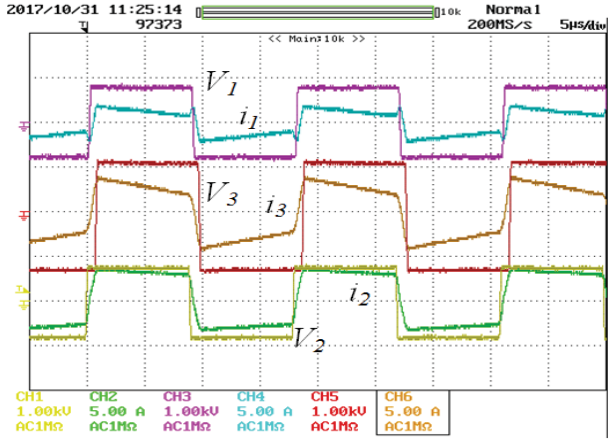

Fig. 10: Fixed Frequency Operation at 50kHz

The efficiency of the converter is measured using power analyzer WT3000. The efficiency is defined as $\eta = \frac{P_{out}}{P_{in}}$. If the RES and ESS both are delivering then $P_{in} = P_1 + P_2$ and $P_{out} = P_3$. If the RES is delivering and ESS charging

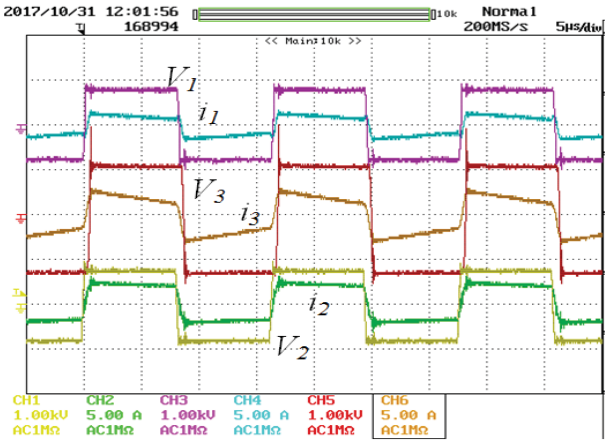

Fig. 11: Variable Frequency Operation at 62kHz

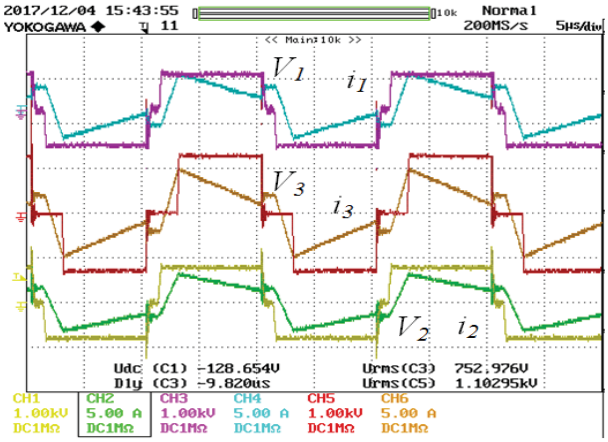

Fig. 12: Quasi-Square Wave Operation for 2kW Operation

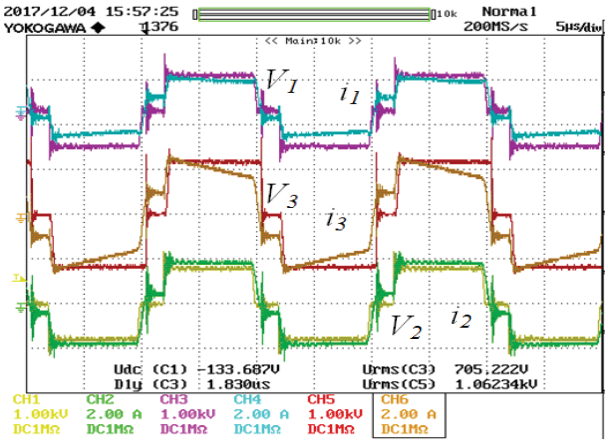

Fig. 13: Quasi-Square Wave Operation for 1.2kW Operation

then $P_{out} = P_3 + P_2$ and $P_{in} = P_1$. It can be observed that using frequency variation, the improvement in efficiency is achieved by a small margin. Using the duty cycle variation method at fixed frequency of 50kHz, the improvement in efficiency achieved is quite considerable. However, the efficiency improvement is achieved around the low power region, while for mid power to full power region, all the three methods provide almost the same efficiency. In figure 12 and 13, it can be observed that few ports have loss of ZVS at very low power region, where only one leg of the converter experiences natural ZVS turn-on.

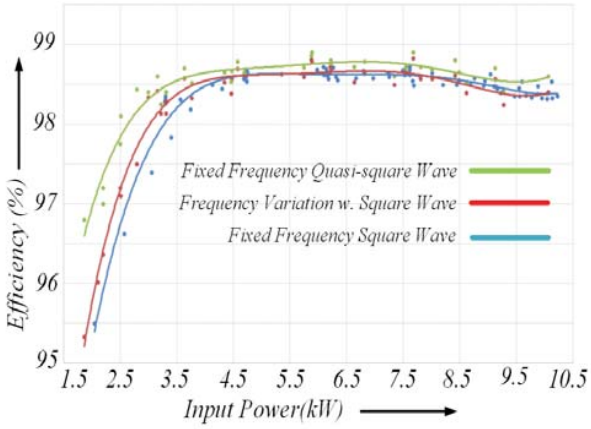

Fig. 14: Converter Efficiency with Different Methods

V. Conclusion

The different methods of operating the three port converter have been successfully tested using the laboratory prototype. The converter models for power flow and loss calculations have been comprehensively defined in sections 2 and 3. The three operating methods provide almost equal efficiency between mid to high power region. The duty cycle variation method provides relatively higher efficiency at low power operating region compared to frequecy variation method.

References

[1] X. She, A.Q. Huang, R. Burgos,"Review of Solid-State Transformer Technologies and Their Application in Power Distribution Systems,"*IEEE Journal of Emerging and Selected Topics in Power Electronics*, 2013, vol. 1, Issue. 3, pp. 186-198.

[2] P. Joebges, J. Hu, R.W.De Doncker"Design method and efficiency analysis of a DAB converter for PV integration in DC grids," *in proc. 2016 IEEE 2nd Annual Southern Power Electronics Conference (SPEC)*, 2016, pp. 1-6.

[3] S.P. Engel, M. Stieneker, N. Soltau, S. Rabiee, H. Stagge, R.W.De Doncker,"Comparison of the Modular Multilevel DC Converter and the Dual-Active Bridge Converter for Power Conversion in HVDC and MVDC Grids" *IEEE Trans. on Power Electronics*, 2015, vol. 30, Issue. 1, pp.124-137.

[4] M.N. Kheraluwala, R.W. Gascoigne, D.M. Divan, E.D. Baumann,"Performance characterization of a high-power dual active bridge DC-to-DC converter,"*IEEE Trans. on Ind. Appl.*, 1992, vol. 28, Issue. 6, pp. 1294-1301.

[5] Z. Chuanhong, J.W. Kolar,"A novel three-phase three-port UPS employing a single high-frequency isolation transformer,"*IEEE 35th Annual Power Electronics Specialists Conference(PESC)*, 2004, pp.4135-4141.

[6] G. Wang, A. Huang, C. Li, "ZVS range extension of 10A 15kV SiC MOSFET based 20kW Dual Active Half Bridge (DHB) DC-DC converter," in *proc. IEEE Energy Conversion Congress and Exposition (ECCE)*, 2012, pp. 1533-1539.

[7] M. Kasper, R.M. Burkart, G. Deboy, J.W. Kolar, "ZVS of Power MOSFETs Revisited," *IEEE Trans. on Power Electronics*, 2016, vol. 31, Issue. 12, pp.8063-8067.

[8] R. Chattopadhyay, S. Bhattacharya, "Modular isolated DC-DC converter with multi-limb transformer for interfacing of renewable energy sources," in *proc. IEEE Applied Power Electronics Conference and Exposition (APEC)*, 2015, pp. 3039-3046.

[9] R. Chattopadhyay, M.A. Juds, P.R. Ohodnicki, S. Bhattacharya, "Modelling, design and analysis of three limb high frequency transformer including transformer parasitics, for SiC Mosfet based three port DAB," in *proc. 42nd Annual Conference of the IEEE Industrial Electronics Societ(IECON)*, 2016, pp. 4181-4186.

[10] R. Chattopadhyay, M.A. Juds, G. Gohil, S. Gulur, P.R. Ohodnicki, S. Bhattacharya, "Optimized design for three port transformer considering leakage inductance and parasitic capacitance," in *proc. IEEE Energy Conversion Congress and Exposition (ECCE)*, 2017, pp. 3247-3254.

[11] R. Chattopadhyay, S. Acharya, G. Gohil, S. Bhattacharya, "One switching cycle current control strategy for triple active bridge phase-shifted DC-DC converter," in *proc. IEEE Industry Applications Society Annual Meeting*, 2017, pp. 1-8.

[12] R. Chattopadhyay, G. Gohil, S. Bhattacharya, "Split-winding type three limb core structured HF transformer for integrating PV and energy storage(ES)," in *proc. IEEE Applied Power Electronics Conference and Exposition (APEC)*, 2017, pp. 2997-3004.

[13] K. Venkatachalam, C.R. Sullivan, T. Abdallah, H. Tacca, "Accurate prediction of ferrite core loss with nonsinusoidal waveforms using only Steinmetz parameters," in *proc. IEEE Workshop on Computers in Power Electronics*, 2002, pp. 36-41.